fibers

MDPI

Article

Experimental Investigation of the Axial Crushing Response of Flax/Glass Eco-Hybrid Self-Supporting Web Composites

Haris Ahmad Israr [1,*], King Jye Wong [1] and Seyed Saeid Rahimian Koloor [2,3,*]

[1] School of Mechanical Engineering, Faculty of Engineering, Universiti Teknologi Malaysia, Johor Bahru 81310, Johor, Malaysia
[2] Institute for Structural Engineering, Department of Civil Engineering and Environmental Sciences, Universität der Bundeswehr München, Werner-Heisenberg-Weg 39, Neubiberg, 85579 Munich, Germany
[3] Department of Aerospace Engineering, Universiti Putra Malaysia, UPM, Serdang 43400, Selangor, Malaysia
* Correspondence: harisahmad@utm.my (H.A.I.); s.s.r.koloor@gmail.com (S.S.R.K.)

Abstract: This study investigates the quasi-static axial crushing tests of eco-hybrid composites based on flax and E-glass fibres strengthened with polyester resin. Five different configurations of self-supporting webs were fabricated to investigate the crushing behaviours of this eco-hybrid composite with different stacking sequences based on intercalation and sandwich-like sequences. The effect of different open-section web profiles was also investigated. The results were plotted in load-displacement curves and the specific energy absorption (SEA), as well as the crushing force efficiency (CFE), were calculated to evaluate the crushing response of each configuration. The test results verified the crushing mechanisms related to the energy absorption depending on the stacking sequence as well as the frontal profile. In this study, all specimens with the intercalation stacking sequence have achieved higher SEA and CFE than specimens with a sandwich-like stacking sequence. In terms of the frontal profile, the sine wave hat shape had the highest CFE, up to 80% compared to other web profiles. Thus, it demonstrated the capability of a sine wave hat-shape eco-composite based on flax fibre to be applied as a crashworthy material.

Keywords: crashworthiness; compressive; flax; eco-composite; self-supporting

Citation: Israr, H.A.; Wong, K.J.; Koloor, S.S.R. Experimental Investigation of the Axial Crushing Response of Flax/Glass Eco-Hybrid Self-Supporting Web Composites. *Fibers* **2022**, *10*, 72. https://doi.org/10.3390/fib10090072

Academic Editors: Ahmad Rashed Labanieh and Vincent Placet

Received: 8 June 2022
Accepted: 22 August 2022
Published: 26 August 2022

1. Introduction

The concept of crashworthiness arose from the observation that many aviation accidents, such as cabin structure collapse, fire, and passenger impact with hard protruding objects, could be avoided [1,2]. This motivated progressive studies in crashworthiness, which are oriented to designing fuel systems, airframes, seat systems, and restraints that can prevent such accidents from occurring, thus making aviation accidents more survivable to help save lives. Crashworthiness is a critical aspect of a vehicle's structural stability and is related to the crash energy-absorbing components [3–5].

The high vertical impact loads during aircraft accidents need to be absorbed in a controlled manner involving the landing gear, seat system, and aircraft subfloor [1]. When considering the ability to absorb kinetic energy [6], a structure must be able to convert the absorbed energy into inelastic energy to prevent accidents from becoming catastrophic, which leads to structural failure and rupture [2,7,8]. In that sense, the aircraft subfloor section is the most important structural component that needs to be designed to limit the deceleration forces due to crash loads and provide post-crash structural integrity to the cabin structure. Early aviation relied on metallic structures to produce such crashworthiness quality as they exhibited considerable capacity in energy absorption and mitigation of impact load. Metals will naturally undergo plastic deformation when subjected to an intense load [9,10]. However, due to the weight constraint, composite materials are progressively replacing metals in aircraft, automobiles, etc., structures [8,11]. Several types

of synthetic fibres used conventionally as reinforcements for composites are carbon fibre, glass fibre, and aramid fibre [11].

Although synthetic fibres are a better alternative to metals in many cases, there are several drawbacks to consider. High material costs, non-recyclability, and pollution are a few of the drawbacks. When brittle type fibres fail, most of them release dust and debris in the crushing zone [12–14]. In addition, synthetic fibres are not environmentally friendly because they cannot be recycled, which has increased the quest for a suitable alternative to other materials [15].

In relation to this concern, natural fibres represent an environmentally sustainable alternative to synthetic fibres. Natural fibres are derived from plants and are renewable by nature with a low level of embodied energy compared to synthetic fibres. Natural fibres such as flax fibres, basalt fibres, and jute fibres exhibit high specific properties, low density, low cost, and are less harmful during handling [16]. However, natural fibres alone are weaker than synthetic fibres, which makes them unsuitable for high-stress applications. Like the alloying of metals, the hybridization of natural fibres with synthetic fibres enhances their material properties. This will result in a notable improvement in the load-carrying capacity of such eco-hybrid composites.

In the open literature, many experimental investigations related to composite crashworthiness studies have been reported, such as different types of fibres [17–19] and resin [20,21], laminate design [19,22,23], trigger configurations [24], geometry [25–27], etc. However, most of these studies used synthetic fibre composites or natural fibre composites, leaving a huge gap in justifying the crashworthiness capability of eco-hybrid composites. Praveen et al. [28] have tried to explore the crashworthiness behaviours of eco-hybrid composite tubes fabricated from epoxy-reinforced glass/kenaf fabrics. Their findings demonstrate that the eco-hybrid composite is more crashworthy than the natural fibre composite [28]. On the other hand, Alkateb et al. have shown that natural flax fibre has great potential to replace synthetic E-glass and mineral-based basalt fibres for crashworthy use [27]. This scenario has motivated this study to examine the crashworthiness behaviour of an eco-hybrid composite made of flax fibre and synthetic glass fibre.

Because of the fuselage subfloor application, it is normally designed with self-supporting web profiles [29]. Besides that, one of the notable advantages of this structure is its ability to self-support without the need for a dedicated test fixture [30], and it is robust to the trigger design [26]. In terms of failure modes, the self-supporting web profiles generally experienced a mixed mode failure, which includes both splaying and fragmentation that could absorb high crash energy. Furthermore, these profiles are also more versatile from the manufacturing standpoint as they are open sections [31]. For that reason, there are several different shapes of self-supporting web profiles reported in the literature, such as hat shapes [30], sine webs [31], and omega [12], due to their ability to maintain stability and continue progressive crushing. For that reason, several configurations of self-supporting web profiles of flax/glass eco-hybrid composites with different geometry and stacking sequences were fabricated to investigate the crushing response under the quasi-static axial crushing tests.

2. Materials and Method

2.1. Specimens

Test specimens were manufactured using hand lay-up. The natural fibre used in this study to form the eco-hybrid composites was Biotex Flax 2 × 2 Twill (Figure 1), supplied by Creative Composite, United Kingdom. As for the synthetic fibre, it was E-glass plain weave fabric (Figure 1) obtained from Chemrex Corporation Sdn. Bhd, 43200 Cheras, Selangor, Malaysia, and all the specimens used polyester resin as the matrix. The flax fibre was selected as it offers low density and cost, high tensile strength and modulus, and availability in the market [32], and based on studies reported in [27,33]. For instance, Meredith et al. [33] compared synthetic carbon fibre with natural fibres including jute, flax, and hemp fibres to understand its energy absorption behaviour. According to the results,

flax fibre was able to achieve higher specific energy absorption (SEA) up to 17.4% than carbon fibre and more than 100% when compared to jute fibre. The properties of the flax fibre, E-glass fibre, and polyester resin were listed in Table 1.

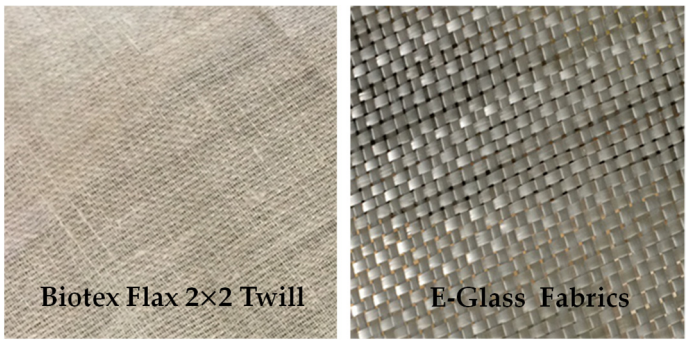

Figure 1. The fibres that are used to form the eco-hybrid composites.

Table 1. Mechanical properties of Flax, E-Glass, and Polyester resin.

Materials	Biotex Flax 2 × 2 Twill [34]	E-Glass Plain Weave Fabrics [34]	Polyester [35]
Arial weight (g/m^2)	200	600	-
Density (g/cm^3)	1.5	2.50	1.2
Tensile modulus (GPa)	40–60	58–68	2–4.5
Ultimate tensile strength, (MPa)	370–630	2000–3500	40–90

To justify the objective of this study, three different self-supporting web moulds, namely 60° hat shape, 90° hat shape, and half-sine hat shape, were prepared. The dimensions of the moulds were set in such a way that the resulting specimens would have a similar frontal area. Figure 2 illustrates the engineering drawing of the frontal shape of each self-supporting web specimen.

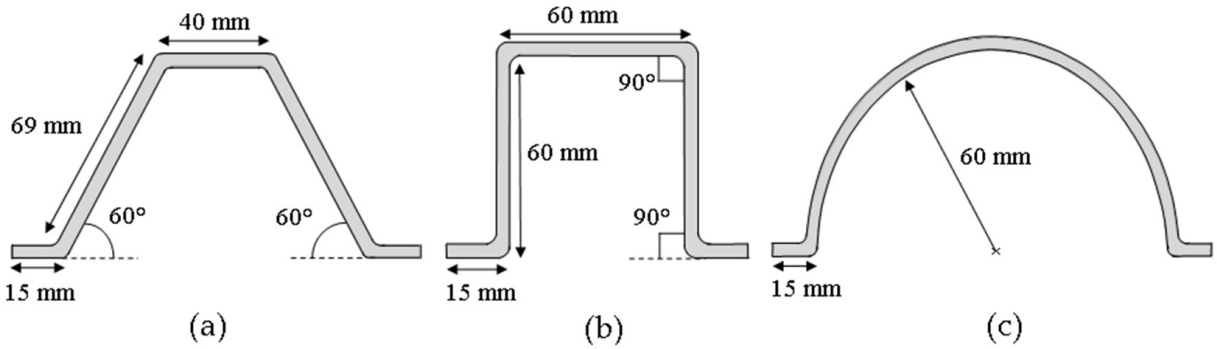

Figure 2. The frontal view of the self-supporting web specimens (**a**) 60° hat-shaped (**b**) 90° hat shape (**c**) half-sine hat shape.

The crushing behaviour of composites is also sensitive to fibre architecture, such as the stacking sequence [16,36,37]. For this reason, two profiles of sandwich-like stacking sequences with different orientations of fibres and one profile with an intercalation stacking sequence were fabricated, and each configuration consists of four test specimens. The illustration of intercalation and sandwich-like layup are presented in Figure 3, and all layers were arranged perpendicular (0° direction) to the metallic base (Figure 4).

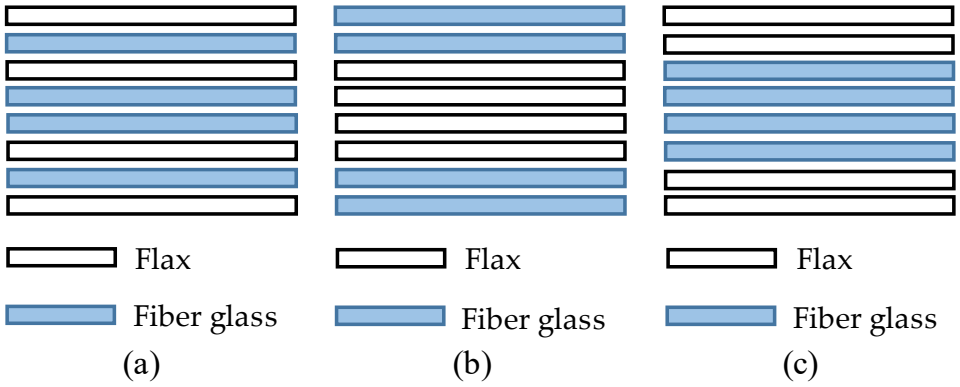

Figure 3. (**a**) The intercalation stacking sequence, (**b**) the sandwich-like stacking sequence with glass fiber as the outmost layer, and (**c**) The sandwich-like stacking sequence with flax fiber as the outmost layer.

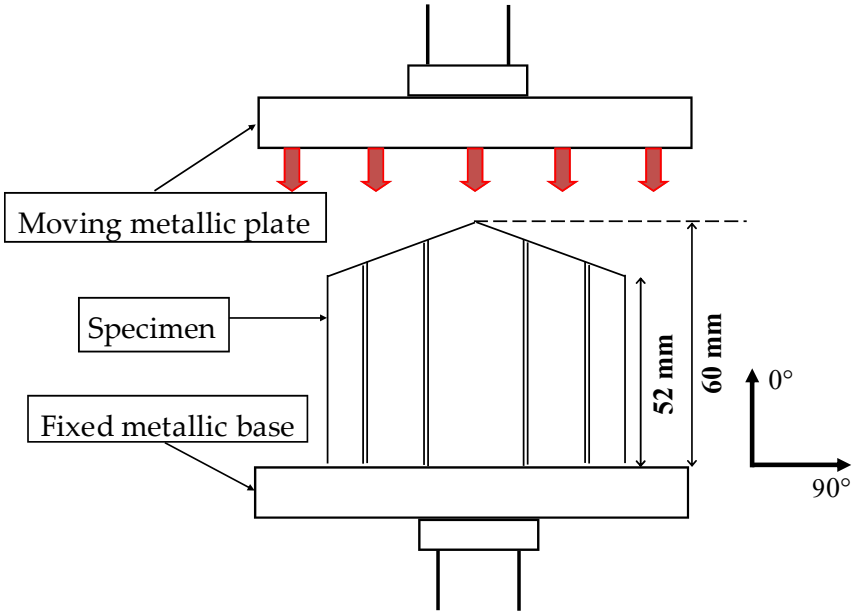

Figure 4. A schematic diagram of the experimental setup.

The manufactured specimens are all listed in Table 2. All three types of self-supporting webs have been manufactured for the intercalation stacking sequence (Figure 3a) to evaluate the impact of frontal profiles that have the same cross-sectional area (IH-60, IH-90, and IH-sine). However, for the sandwich-like stacking sequence (Figure 3b,c), only a 60° hat-shaped web has been constructed (S-H-60-F and SH-60-G) to investigate the effects of the stacking sequence alongside specimen IH-60.

Additionally, the top of the crushed specimen was shaped to form a tulip-type trigger (Figure 4), a design that many researchers have employed to support a persistent crushing mode of failure. Palanivelu et al. [38] mentioned that different levels of energy absorption could be achieved by changing the structural geometry while keeping the other variables constant for all tested composites. Although there were minor variations as indicated by the coefficient of variation (c.v) as shown in Table 2, factors such as thickness, volume, and mass of the specimens were treated as constant variables in this investigation.

Table 2. Details of specimen configurations.

Stacking Sequence	Average Thickness (mm) (c.v%)	Average Mass (g) (c.v%)	Volume Fraction Fibre, V_f	Volume Fraction Matrix, V_m	No. of Specimen
Intercalation:					
IH-60	4.14 (0.29)	66.32 (1.09)	0.47	0.53	4
IH-90	4.12 (0.28)	66.21 (1.07)	0.47	0.53	4
IH-sine	4.15 (0.3)	62.55 (0.81)	0.46	0.54	4
Sandwich-like:					
SH-60-F	4.14 (0.27)	59.21 (1.3)	0.46	0.54	4
SH-60-G	4.13 (0.29)	65.3 (0.86)	0.48	0.52	4

Note: I = intercalation, H = hat shape, S = sandwich like shape, F = flax, G = glass fibre, c.v = coefficient of variation.

2.2. Experimental Test

In this study, all the specimens were tested under quasi-static crushing tests at a constant low loading rate. Thus, the test is easy to control and allows one to precisely observe the crushing processes and damage mechanisms, as reported by many authors [12,13,39]. The test was performed using the Instron 600DX machine located in the Solid Mechanics Laboratory at Universiti Teknologi Malaysia (UTM).

In this test, the metallic base of the machine was fixed, and the moving metallic plate was axially displaced at a constant loading rate of 5 mm/min, the same loading rate imposed in [28]. Figure 4 depicts the test setup and specimen location. A maximum of 30 mm of crushing extension was set as the standard length of crushing for every specimen, which is considered sufficient for progressive crushing.

The load-displacement data for each test was recorded and acquired at a rate of 100 Hz using the Instron 600DX automatic data acquisition system. Then, the total energy absorption of different configurations was calculated by considering a deformation length of 30 mm for all specimens tested. The specific energy absorption (SEA) was calculated using Equation (1) to assess the effectiveness of each configuration in terms of energy absorption capability:

$$SEA = \frac{E_{plateau}}{M_{crush}} = \frac{P_{avg}}{\rho_A}, \quad (1)$$

where $E_{plateau}$ is the energy absorbed in the crushing plateau, M_{crush} is the mass of the crushed material, ρ is the density of the material, A is the cross-sectional area, and P_{avg} is the average crushing load sustained by the specimens during the progressive crushing process.

Similarly, the average peak loads and average crushing loads of each configuration were determined from the load-displacement curve to calculate the respective configuration's crash force efficiency (CFE) using the formula as follows:

$$\mathrm{CFE} = \frac{\mathrm{P_{avg}}}{\mathrm{P_{max}}} \times 100\%, \quad (2)$$

where $\mathrm{P_{max}}$ is the maximum peak load sustained by the specimens during the crushing initiation process.

3. Result and Discussion

The crushing behaviour of the tested specimens will be discussed in terms of load-displacement curve, failure mechanisms, and crashworthiness properties.

3.1. Load-Displacement Curve

Figure 5 illustrates an example of axial crushing load-displacement curves of quasi-static crushing tests of all four samples of the IH-60 configuration. The crushing processes of all four samples started from the trigger surface of the samples, which caused a gradual increment of compressive load with respect to crushing extension. All four samples sustained a peak crushing load as they approached a crushing extension of 10 mm on average during the initiation process (Zone I). The crushing process started to fluctuate with a small difference in crushing load, which symbolized the progressive crushing process (Zone II), during which the fibres started to experience sustainable local fragmentation. At this stage, the behaviour of each test sample varied slightly among each other, depending on the number of fibres having local fragmentation [13]. The compressive load applied also caused the buckling of specimens to grow, which resulted in a significant drop in compressive load towards the end of the experiment. This is known as the end of the crushing process (Zone III).

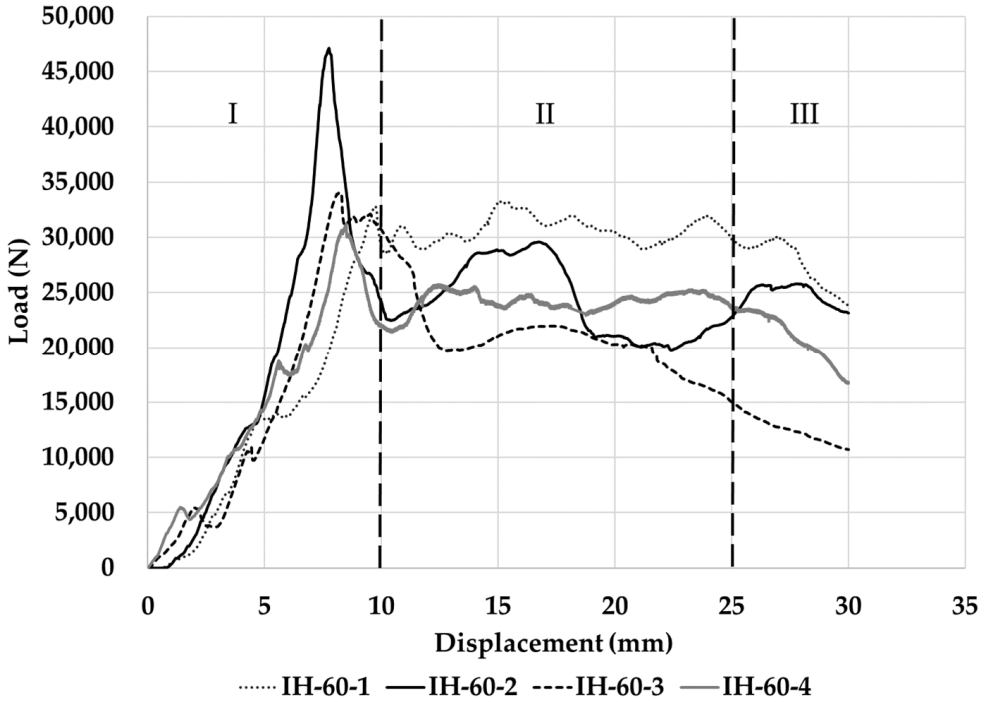

Figure 5. An example of axial crushing load-displacement curves of all four samples IH-60 configuration.

The axial crushing load-displacement curves for other configurations of self-supporting webs are depicted in Figure 6a,b, respectively, for webs with different frontal profiles and different stacking sequences. There is only one representative of each of the four samples of each configuration in both figures. Despite having varied frontal profiles (Figure 6a) and stacking sequences (Figure 6b), all of the studied specimen samples went through the same three major crushing stages, which are crush initiation (Zone I), progressive crushing (Zone II), and the end of crush (Zone III), respectively. The same crushing stages and observations can also be found in [13,39,40]. The consistency of the crushing stages demonstrates that the presence of a tulip-type triggering mechanism is effective in preventing the global buckling failure mode.

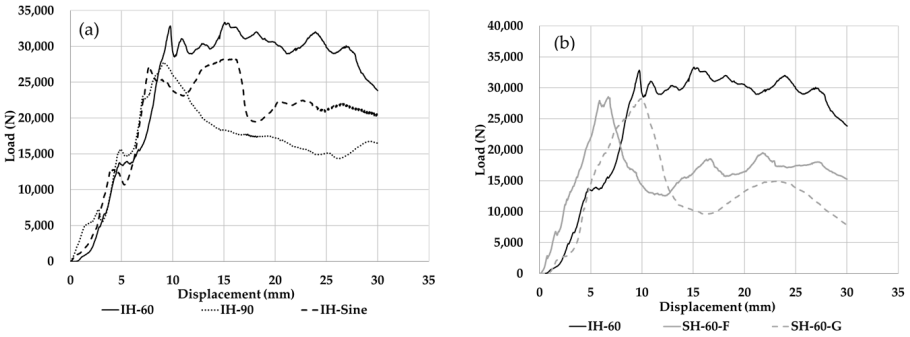

Figure 6. The axial crushing load-displacement response for (**a**) webs having different frontal profiles, and (**b**) webs having different stacking sequences.

3.2. Failure Mechanism

The crushing morphologies of Zone I, Zone II, and Zone III for all configurations are displayed in Figure 7. Most of the configurations were crushed with the progressive folding mode, comprising buckling, local fragmentation, and some splaying modes. It can be noticed that in Figures 5 and 6, most of the configurations sustained peak crushing load as they approached a crushing extension of between 7 and 10 mm on average during the initiation process (Zone I). At this stage, the tip (trigger surface) of the sample is crushed with local fragmentation, and the load grows as the direct contact area between the sample and the metallic base increases [13,40].

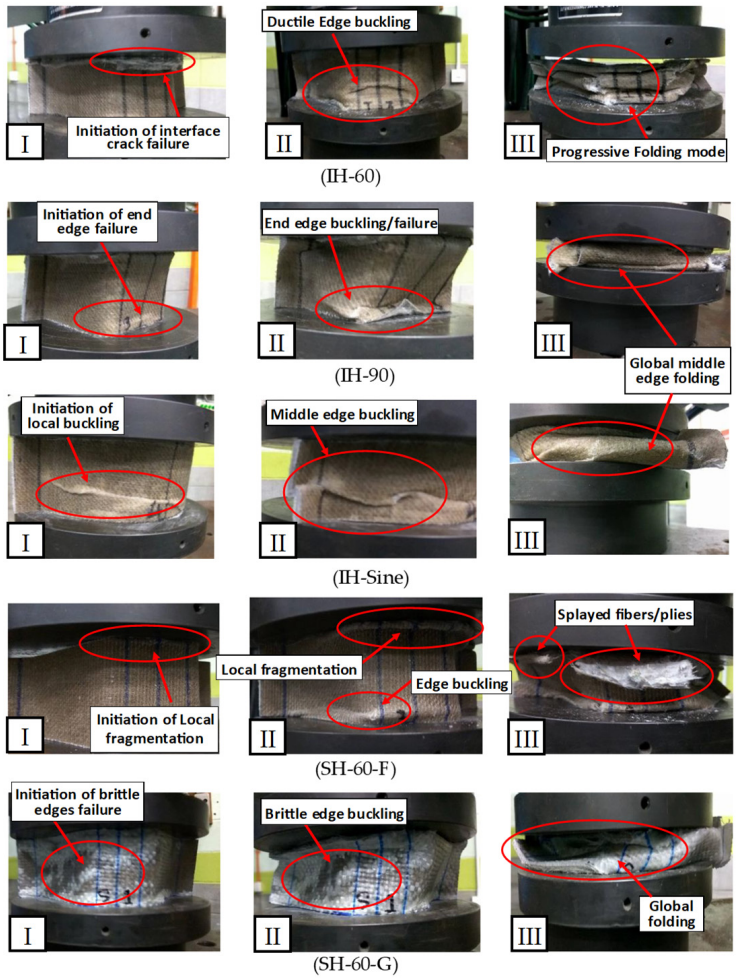

Figure 7. The crushing morphology at each stage of crushing (I: Zone I) (II: Zone II) (III: Zone III).

Then, the interlaminar crack appears to have caused some fibres to splay due to high transverse shear stress in interfaces, leading to a severe drop in the force (image of Zone II in Figure 7). Besides that, from the physical observations made during the testing, some of the configurations, such as IH-60, SH-60-G, and SH-60-F (Figure 7), experienced buckling about the edges that caused a drop in compressive load after achieving their peak crushing loads in their respective cases. There was visible debris from glass fibsre layers as a result of the local fragmentation during the progressive crushing process. As predicted, the SH-60-G configuration produced the highest volume of debris compared to other configurations, as the outer layers of SH-60-G samples are brittle by nature.

At the end of the crushing process (Zone III), the SH-60-F and SH-60-G configurations were crushed by a combination of splaying and folding modes, with the splaying mode dominant, as shown in Figure 7 (Zone III). While for intercalation specimens (IH-60, IH-90, and IH-Sine), the crushing process was dominated by the folding mode. Moreover, it can be noticed that the number of fractured plies and interlaminar cracks of the samples stacked with intercalation sequences was smaller compared to samples with the sandwich-like sequence.

3.3. Energy Absorption Behaviour

Table 3 presents the average results obtained from testing on four samples of each configuration under axial crushing. The average results were used for the discussion as the testing results showed that the coefficient of variation (c.v.) of these crashworthiness measures was relatively low and acceptable, i.e., less than 20%.

Table 3. Average results of the axial crushing test of each configuration.

Stacking Sequence	Density (g/cm^3) (c.v%)	Peak Load (kN) (c.v%)	Average Crushing Load (kN) (c.v%)
Intercalation:			
IH-60	1.44 (1.09)	36.32 (17.5)	24.75 (15.5)
IH-90	1.48 (1.07)	26.93 (6.5)	18.04 (17.4)
IH-Sine	1.39 (0.81)	25.87 (10.5)	20.84 (14.9)
Sandwich like:			
SH-60-F	1.42 (0.86)	29.06 (8.9)	16.94 (13.5)
SH-60-G	1.37 (1.3)	29.18 (17.9)	13.75 (10.6)

A leading parameter used as a comparative tool is the average crushing load (P_{avg}) sustained by the samples during the progressive crushing process. The average crushing load of specimens with different frontal profiles and stacking sequences was compared respectively. In terms of the effect of frontal profiles, Table 3 and Figure 6a demonstrates that IH-60 specimens with respect to IH-sine and IH-90 configurations sustained a much higher average crushing load of approximately 19% and 37%, respectively. While regarding the impact of the stacking sequence, the intercalation stacking sequence may withstand more local fragmentation during progressive crushing (zone II) than sandwich-like stacking sequences (SH-60-F and SH-60-G) up to a maximum of 80%, according to Table 3 and Figure 6b.

To evaluate the effectiveness of each configuration with respect to energy absorption capability, the SEA was calculated, as shown in Figure 8. Although the thickness of all configurations was almost similar, the energy absorption behaviour of each configuration differs from one to another. The difference in SEA is mainly due to the different structural geometry of frontal profiles and the difference in the stacking sequence arrangement. When comparing IH-60 specimens (20.36 kJ/kg) to IH-Sine (18.33 kJ/kg) and IH-90 (14.45 kJ/kg)

for frontal profiles effects (Figure 8a), it can be noted that IH-60 specimens managed to demonstrate the greatest SEA value with more than 11% and 40.8 percent, respectively. While Figure 8b illustrates the effect of stacking sequence on SEA, it can be seen clearly that the intercalation stacking sequence had better SEA as it showed an additional 28% and 74%, respectively, with respect to sandwich-like stacking sequences (SH-60-F and SH-60-G).

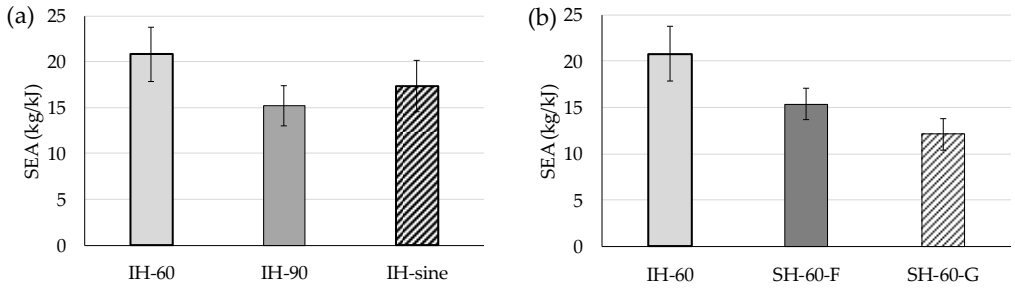

Figure 8. The average results of SEA for (**a**) webs having different frontal profiles and (**b**) webs having different stacking sequences.

Besides that, the SEA values of the same frontal profile, which was made of a sandwich-like stacking sequence (SH-60-F and SH60-G), recorded a significant difference in SEA values due to the arrangement of the flax and glass fibres. The difference in fibre arrangement has caused the SH-60-F to absorb 36% more energy per kg compared to the SH-60-G. This is because the outer layer of SH-60-G samples, which were made of a glass fibre layer, is brittle, making them collapse easily when subjected to compressive load as observed during the tests. Nevertheless, these average SEA values generally are comparable to other SEA values of synthetic composite materials with different geometric configurations that can be obtained in the open literature, such as woven fabric CFRP (1526 kJ/kg) [41], braided carbon (15–30 kJ/kg) [42], kevlar49/epoxy (25 kJ/kg) [43].

In this study, the frontal profile and the stacking sequence also affected the peak crushing load. As shown in Table 3, the IH-60 configuration exhibited the highest peak load of up to 34.8% (IH-90) and 40.4% (IH-sine), respectively, when considering the effect of frontal profiles, and exhibited more than 24% (SH-60-F and SH-60-G) when considering the effect of stacking sequence arrangements. From Table 2, it is noticeable that the IH-Sine specimens, which produced the second-highest SEA value (Figure 8), exhibited the lowest average peak crushing load (25.87 kN) compared to the other configurations. A similar trend was remarked in a study done by Palanivelu et al. [38]. In fact, a lower peak crushing load is more desirable in crashworthy structures as it may contribute to easier deformation during the crash events and the magnitude of peak load transferred to primary structures could be minimized [38]. In short, the average peak load result is heavily influenced by structural geometry and does not carry a direct proportionality to the corresponding SEA value.

The last result to be discussed in this study related to energy absorption behaviour is the CFE, which is the ratio between the average crushing load and the peak crushing load. This result is important to identify the optimum energy absorber among the tested configurations as presented in Figure 9. The result shows that the IH-Sine configuration produced the highest efficiency (80.57%) compared to IH-60 (67.03%), followed by IH-90 (66.98%)., SH-60-F (58.3%), and SH-60-F (47.12%) configurations, respectively. It reveals that among the studied frontal profiles, the IH-Sine configuration has a better uniformity of crushing load in absorbing the crash energy. For instance, as shown in Figure 9a, it delivered more than 20% compared to other frontal profiles. According to the results presented in Figure 9b, the intercalation stacking sequence (IH-60), as compared to the sandwich-like stacking sequence, has a better crushing efficiency of more than 15%.

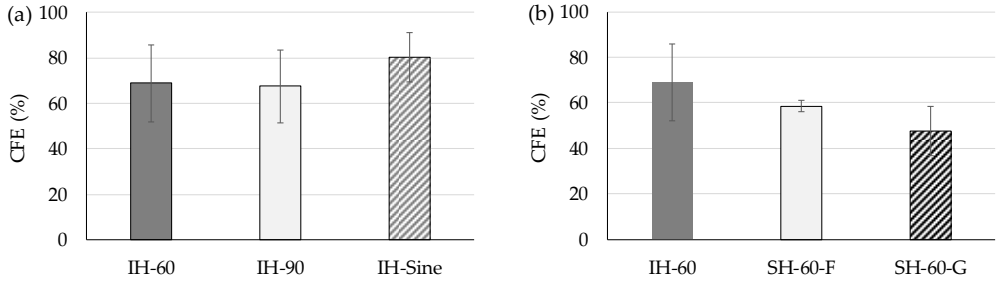

Figure 9. The average results of CFE for (**a**) webs having different frontal profiles and (**b**) webs having different stacking sequences.

4. Conclusions

The crashworthiness behaviour of eco-hybrid composites based on flax and E-glass fibres has been investigated with five different configurations to study the effects of frontal geometry as well as the stacking sequence. It can be concluded that the frontal geometry with a 60° hat shape (IH-60) has the capability to exhibit the highest SEA compared to other frontal profiles. Nevertheless, it has less crushing efficiency when compared to the sine wave-hat shape profile (IH-Sine), which has better crushing load homogeneity. In terms of stacking sequence, it appears that applying the intercalation stacking sequence would be more favorable to produce an eco-hybrid composite for the self-supporting structure that has better energy absorption behaviour with higher SEA as well as higher crushing efficiency when compared to the sandwich-like stacking sequence. The study also revealed the significance of fibre arrangement in the stacking sequence to produce the eco-hybrid composite. This was proven through the comparison between SH-60-G and SH-60-F configurations, where samples with a sandwich-like stacking sequence that had flax as their outer layer sustained higher SEA compared to the specimen fabricated with glass fibre as the outer layer. The result also proved the ability of flax fibres to hold the composite shape together, as the SH-60-F configuration produced less debris at the crushing area compared to the SH-60-G configuration. This result renders it a suitable material to be used in the outer layers rather than brittle glass fibre.

Finally, the sine-hat shape with intercalation stacking sequence can be regarded as the optimum energy absorber among the investigated configurations since it produced the highest crushing efficiency, which is desirable behaviour for any crashworthy component in vehicle structural design.

Author Contributions: Conceptualization, and Data curation H.A.I.; Formal analysis, Investigation and Methodology H.A.I., K.J.W. and S.S.R.K., Resources, H.A.I., Funding acquisition, S.S.R.K.; Project administration, H.A.I. and S.S.R.K.; Supervision, H.A.I.; Validation, and Visualization, H.A.I., K.J.W. and S.S.R.K.; Writing—original draft, H.A.I.; Writing—review & editing, H.A.I., K.J.W. and S.S.R.K. All authors have read and agreed to the published version of the manuscript.

Funding: The authors acknowledge Universiti Teknologi Malaysia and the Ministry of Education for the financial support through the UTM-TDR Grant No. 05G22 and FRGS Grant No. 4F727.

Institutional Review Board Statement: Not applicable.

Acknowledgments: The authors highly acknowledge Universiti Teknologi Malaysia and the Ministry of Education Malaysia for the financial support through the UTM-TDR grant, No. 05G22, and FRGS grant, No. 4F727. The research was partially supported by Universiti Teknologi Malaysia through grant number Q.J130000.21A6.00P39.

Conflicts of Interest: The authors declare no conflict of interest.

References

1. Bisagni, C. Crashworthiness of helicopter subfloor structural components. *Aircr. Eng. Aerosp. Technol.* **1999**, *71*, 6–11. [CrossRef]
2. Farokhi Nejad, A.; Alipour, R.; Shokri Rad, M.; Yazid Yahya, M.; Rahimian Koloor, S.S.; Petrů, M. Using Finite Element Approach for Crashworthiness Assessment of a Polymeric Auxetic Structure Subjected to the Axial Loading. *Polymers* **2020**, *12*, 1312. [CrossRef]
3. Bisagni, C.; Di Pietro, G.; Fraschini, L.; Terletti, D. Progressive crushing of fiber-reinforced composite structural components of a Formula One racing car. *Compos. Struct.* **2005**, *68*, 491–503. [CrossRef]
4. Obradovic, J.; Boria, S.; Belingardi, G. Lightweight design and crash analysis of composite frontal impact energy absorbing structures. *Compos. Struct.* **2012**, *94*, 423–430. [CrossRef]
5. Costas, M.; Diaz, J.; Romera, L.; Hernandez, S.; Tielas, A. Static and dynamic axial crushing analysis of car frontal impact hybrid absorbers. *Int. J. Impact Eng.* **2013**, *62*, 166–181. [CrossRef]
6. Joshani, M.; Koloor, S.; Abdullah, R. Damage Mechanics Model for Fracture Process of Steel-Concrete Composite Slabs. *Appl. Mech. Mater.* **2012**, *165*, 339–345. [CrossRef]
7. Abdi, B.; Koloor, S.S.R.; Abdullah, M.R.; Amran, A.; Yahya, M.Y. Effect of Strain-Rate on Flexural Behavior of Composite Sandwich Panel. In *Applied Mechanics and Materials*; Trans Tech Publications Ltd.: Frienbach, Switzerland, 2012; Volume 229–231, pp. 766–770.
8. Kashyzadeh, K.; Koloor, S.R.; Bidgoli, M.O.; Petrů, M.; Asfarjani, A.A. An Optimum Fatigue Design of Polymer CompositeCompressed Natural Gas Tank Using Hybrid Finite Element-Response Surface Methods. *Polymers* **2021**, *13*, 483. [CrossRef]
9. Bambach, M. Axial capacity and crushing of thin-walled metal, fibre–epoxy and composite metal–fibre tubes. *Thin-Walled Struct.* **2010**, *48*, 440–452. [CrossRef]
10. Wang, X.; Zheng, Z.; Yu, J. Crashworthiness design of density-graded cellular metals. *Theor. Appl. Mech. Lett.* **2013**, *3*, 031001. [CrossRef]
11. Nejad, A.F.; Bin Salim, M.Y.; Koloor, S.S.R.; Petrik, S.; Yahya, M.Y.; Abu Hassan, S.; Shah, M.K.M. Hybrid and Synthetic FRP Composites under Different Strain Rates: A Review. *Polymers* **2021**, *13*, 3400. [CrossRef]
12. Jackson, A.; Dutton, S.; Gunnion, A.; Kelly, D. Investigation into laminate design of open carbon–fibre/epoxy sections by quasi–static and dynamic crushing. *Compos. Struct.* **2011**, *93*, 2646–2654. [CrossRef]
13. Israr, H.; Rivallant, S.; Barrau, J. Experimental investigation on mean crushing stress characterization of carbon–epoxy plies under compressive crushing mode. *Compos. Struct.* **2013**, *96*, 357–364. [CrossRef]
14. Boria, S.; Scattina, A.; Belingardi, G. Axial energy absorption of CFRP truncated cones. *Compos. Struct.* **2015**, *130*, 18–28. [CrossRef]
15. Saba, A.M.; Khan, A.H.; Akhtar, M.N.; Khan, N.A.; Koloor, S.S.R.; Petrů, M.; Radwan, N. Strength and flexural behavior of steel fiber and silica fume incorporated self-compacting concrete. *J. Mater. Res. Technol.* **2021**, *12*, 1380–1390. [CrossRef]
16. Jusoh, M.S.M.; Santulli, C.; Yahya, M.Y.M.; Hussein, N.S.; Ahmad, H.A.I. Effect of stacking sequence on the tensile and flexural properties of glass fibre epoxy composites hybridized with basalt, flax or jute fibres. *Mater. Sci. Eng. Adv. Res.* **2016**, *1*, 19–25.
17. Kim, J.-S.; Yoon, H.-J.; Shin, K.-B. A study on crushing behaviors of composite circular tubes with different reinforcing fibers. *Int. J. Impact Eng.* **2011**, *38*, 198–207. [CrossRef]
18. Ochelski, S.; Gotowicki, P. Experimental assessment of energy absorption capability of carbon-epoxy and glass-epoxy composites. *Compos. Struct.* **2009**, *87*, 215–224. [CrossRef]
19. Yan, L.; Wang, B.; Kasal, B. Can Plant-Based Natural Flax Replace Basalt and E-Glass for Fiber-Reinforced Polymer Tubular Energy Absorbers? A Comparative Study on Quasi-Static Axial Crushing. *Front. Mater.* **2017**, *4*, 42. [CrossRef]
20. Ramakrishna, S. Microstructural design of composite materials for crashworthy structural applications. *Mater. Des.* **1997**, *18*, 167–173. [CrossRef]
21. Hamada, H.; Ramakrishna, S.; Satoh, H. Crushing mechanism of carbon fibre/PEEK composite tubes. *Composites* **1995**, *26*, 749–755. [CrossRef]
22. Hull, D. A unified approach to progressive crushing of fibre-reinforced composite tubes. *Compos. Sci. Technol.* **1991**, *40*, 377–421. [CrossRef]
23. Ismail, A.E. Axial crushing energy absorption capability of steel/kenaf fibre hybrid cylindrical tubes. *Int. J. Eng. Technol.* **2015**, *7*, 1098–1104.
24. Eshkoor, R.; Ude, A.; Oshkovr, S.; Sulong, A.; Zulkifli, R.; Ariffin, A.; Azhari, C. Failure mechanism of woven natural silk/epoxy rectangular composite tubes under axial quasi-static crushing test using trigger mechanism. *Int. J. Impact Eng.* **2014**, *64*, 53–61. [CrossRef]
25. Jiménez, M.; Miravete, A.; Larrodé, E.; Revuelta, D. Effect of trigger geometry on energy absorption in composite profiles. *Compos. Struct.* **2000**, *48*, 107–111. [CrossRef]
26. Feraboli, P.; Wade, B.; Deleo, F.; Rassaian, M. Crush energy absorption of composite channel section specimens. *Compos. Part A Appl. Sci. Manuf.* **2009**, *40*, 1248–1256. [CrossRef]
27. Alkateb, M.; Sapuan, S.; Leman, Z.; Ishak, M.; Jawaid, M. Vertex angles effects in the energy absorption of axially crushed kenaf fibre-epoxy reinforced elliptical composite cones. *Def. Technol.* **2018**, *14*, 327–335. [CrossRef]
28. Kumar, A.P.; Shunmugasundaram, M.; Sivasankar, S.; Sankar, L.P. Static axial crushing response on the energy absorption capability of hybrid Kenaf/Glass fabric cylindrical tubes. *Mater. Today Proc.* **2020**, *27*, 783–787.

29. Farley, G.L. *Energy-Absorption Capability of Composite Tubes and Beams*; Virginia Polytechnic Institute and State University: Blacksburg, VA, USA, 1989.
30. Joosten, M.; Dutton, S.; Kelly, D.; Thomson, R. Experimental and numerical investigation of the crushing response of an open section composite energy absorbing element. *Compos. Struct.* **2011**, *93*, 682–689. [CrossRef]
31. Feraboli, P. Development of a Corrugated Test Specimen for Composite Materials Energy Absorption. *J. Compos. Mater.* **2008**, *42*, 229–256. [CrossRef]
32. Yan, L.; Chouw, N.; Jayaraman, K. Flax fibre and its composites—A review. *Compos. Part B* **2014**, *56*, 296–317. [CrossRef]
33. Meredith, J.; Ebsworth, R.; Coles, S.; Wood, B.M.; Kirwan, K. Natural fibre composite energy absorption structures. *Compos. Sci. Technol.* **2012**, *72*, 211–217. [CrossRef]
34. Jusoh, M.S.M.; Israr, H.A.; Yahya, M.Y. Indentation and Low Velocity Impact Properties of Woven E-glass Hybridization with Basalt, Jute and Flax Toughened Epoxy Composites. In Proceedings of the 3rd International Conference on Power Generation systems and Renewable Energy Technologies, IEEE, Johor Bahru, Malaysia, 4–6 April 2017; pp. 164–168.
35. Wong, K.; Low, K.; Israr, H. Impact resistance of short bamboo fibre reinforced polyester concretes. *Proc. Inst. Mech. Eng. Part L J. Mater. Des. Appl.* **2015**, *231*, 683–692. [CrossRef]
36. Jusoh, M.S.M.; Yahya, M.Y.M.; Mustafa, Z.; Ahmad, H.A.I. Effect of layering pattern on mechanical and water absorption properties of glass/flax reinforced epoxy. *J. Teknol.* **2017**, *79*. [CrossRef]
37. Muralidhar, B. Tensile and compressive properties of flax-plain weave preform reinforced epoxy composites. *J. Reinf. Plast. Compos.* **2013**, *32*, 207–213. [CrossRef]
38. Palanivelu, S.; VAN Paepegem, W.; Degrieck, J.; Kakogiannis, D.; Van Ackeren, J.; Van Hemelrijck, D.; Wastiels, J.; Vantomme, J. Comparative study of the quasi-static energy absorption of small-scale composite tubes with different geometrical shapes for use in sacrificial cladding structures. *Polym. Test.* **2010**, *29*, 381–396. [CrossRef]
39. Joosten, M.; Hirth, C.; Thomson, R.; Koerber, H. Effect of environmental conditions on the failure mechanisms and energy absorption of open-section crush elements under quasi-static loading. *Compos. Struct.* **2019**, *209*, 747–753. [CrossRef]
40. Ren, Y.; Jiang, H.; Liu, Z. Evaluation of double- and triple-coupled triggering mechanisms to improve crashworthiness of composite tubes. *Int. J. Mech. Sci.* **2019**, *157*, 1–12. [CrossRef]
41. Zhao, X.; Zhu, G.; Zhou, C.; Yu, Q. Crashworthiness analysis and design of composite tapered tubes under multiple load cases. *Compos. Struct.* **2019**, *222*, 110920. [CrossRef]
42. Xiao, X.; McGregor, C.; Vaziri, R.; Poursartip, A. Progress in braided composite tube crush simulation. *Int. J. Impact Eng.* **2009**, *36*, 711–719. [CrossRef]
43. Farley, G.L.; Jones, R.M. Analogy for the Effect of Material and Geometrical Variables on Energy-Absorption Capability of Composite Tubes. *J. Compos. Mater.* **1992**, *26*, 78–89. [CrossRef]